

## Electronic Supporting Information (ESI)

### **A Co(II)-Coordination Polymer for Ultrahigh Superprotonic Conduction: An atomistic Insight through Molecular Simulations and QENS Experiments**

*Shyam Chand Pal<sup>a</sup>, Santanu Chand<sup>a</sup>, Anaparthi Ganesh Kumar<sup>b</sup>, Paulo G. M. Mileo<sup>c</sup>, Ian Silverwood<sup>d</sup>, Guillaume Maurin<sup>c</sup>, Susanta Banerjee<sup>b</sup>, Syed Meheboob Elahi<sup>a</sup> and Madhab C. Das<sup>\*a</sup>*

<sup>a</sup>Department of Chemistry, Indian Institute of Technology Kharagpur, Kharagpur-721302, India.

<sup>b</sup>Materials Science Centre, Indian Institute of Technology Kharagpur, Kharagpur -721302, India.

<sup>c</sup>Institut Charles Gerhardt, Montpellier UMR 5253 CNRS ENSCM UM, Université Montpellier, 34095 Montpellier CEDEX 05, France.

<sup>d</sup>ISIS Neutron and Muon Facility, Science and Technology Facilities Council, Rutherford Appleton Laboratory, Harwell Science and Innovation Campus, Oxon OX11 0QX.

**Materials and General Instrumentations:** All the reagents were commercially available and used without further purification. Distilled water was used throughout the synthesis. The ATR IR spectra were recorded in the range of 400-4000 cm<sup>-1</sup> on a Perkin-Elmer RX1 spectrophotometer. PXRD patterns were recorded using Cu K<sub>α</sub> radiation (1.5418 Å) on a Bruker D8 Advance diffractometer. Thermogravimetric analysis (TGA) was performed using a TG 209 F3 Tarsus (Netzsch) and the sample was heated from room temperature to 800 °C at a rate of 5 °C min<sup>-1</sup> under N<sub>2</sub> atmosphere. Differential scanning calorimetry (DSC) were performed using Perkin Elmer Pyris Diamond DSC under N<sub>2</sub> atmosphere.

#### **Experimental Section**

##### **Synthesis of {[Co (bpy)<sub>3</sub>(H<sub>2</sub>O)<sub>2</sub>] (bpy) · 2NO<sub>3</sub> · (5.4 H<sub>2</sub>O)}<sub>n</sub>, PCM-1**

Co(NO<sub>3</sub>)<sub>2</sub>·6H<sub>2</sub>O (0.291 g, 1.00 mmol) and bpy (0.156 g, 1.00 mmol) was added to a 25 ml of distilled water and stirred the solution for 30 min in hot condition. After that the solution was filtered and filtrate part kept for slow evaporation. Within 7 days deep red block shape X-ray quality crystals of **PCM-1** was separated. Yield: 0.467 g (0.5 mmol, 50%). Elemental analysis calculated for C<sub>40</sub> H<sub>46.8</sub> Co N<sub>10</sub> O<sub>13.4</sub>: C, 51.40; H, 5.06; N, 14.99. Found (%) C, 51.32; H, 5.10; N, 15.01. IR (ATR IR, cm<sup>-1</sup>) 3404, 1610, 1533, 1335, 1211, 1064, 1002, 801, 620.

**Single Crystal X-ray Diffraction.** The crystal and refinement data for **PCM-1** was collected in Table S1. In this case, a crystal of appropriate size was selected from the mother liquor and

immersed in paratone oil and then it was mounted on the tip of a glass fiber and cemented using epoxy resin. Single crystal X-ray data were collected at 100 K on a Bruker SMART APEX II CCD diffractometer using graphite-monochromated Mo-K $\alpha$  radiation (0.71073 Å). The linear absorption coefficients, scattering factors for the atoms and the anomalous dispersion corrections were taken from International Tables for X-ray Crystallography. The data integration and reduction were processed with SAINT<sup>1</sup> software. An empirical absorption correction was applied to the collected reflections with SADABS using XPREP.<sup>2</sup> The structure was solved by the direct method using SHELXTL and was refined on F<sup>2</sup> by full-matrix least-squares technique using the SHELXL-2014<sup>3</sup> program package. For all the cases non-hydrogen atoms were refined anisotropically. The hydrogen atoms on the coordinated water molecule could be assigned from Difference Fourier map. All other hydrogen atoms are geometrically fixed using riding atom model. Selected bond lengths and bond angles are listed in Table S2. The solvent accessible voids space in **PCM-1** are occupied by large no of disordered nitrate and water molecule, no satisfactory disorder model could be achieved and therefore *PLATON/SQUEEZE*<sup>4</sup> routine was used to remove these electron densities. The final formula of **PCM-1** was derived from the squeeze result combined with the elemental analysis and TGA data. The *SQUEEZE* result (117.8 electrons calculated using *PLATON* Software) suggests that there are 2 NO<sub>3</sub><sup>-</sup> and 5.4 H<sub>2</sub>O molecules located in the cavity per unit cell (116.0 electrons) which is well consistent with the elemental analysis and TGA results.

### **Proton conduction Analysis**

The proton conductivity of compacted pellet of the powdered sample were evaluated by the electrochemical impedance spectroscopy (EIS) using Gamry Instruments, Reference 3000 galvanostat between frequency range of 100 Hz to 1 MHz. The pellets were prepared using 100 mg of bulk samples was compressed under a pressure of 500 MPa (**PCM-1**: 1.4 cm width and 0.062 cm in thickness) and exposed to controlled humidity environments for 24 hours. Proton conductivity was calculated using the following equation:

$$\sigma = \frac{l}{(RA)}$$

Where  $\sigma$  is in plane proton conductivity in S cm<sup>-1</sup>,  $l$  is the distance between the two electrodes (here, 0.425 cm),  $R$  is the measured resistance of the samples and  $A$  is an area of the sample i.e., width (cm)  $\times$  thickness (cm) of the samples. The proton conductivity of the pellet sample

at different humidity was measured using a HSA humidifier unit and an FC-25-01-BT conductivity cell from Electrochem, Inc.

Activation energy (Ea) for the materials conductivity was estimated from the following equation:

$$\sigma T = \sigma_0 \exp(-E_a/k_b T)$$

where  $\sigma$  is the proton conductivity,  $\sigma_0$  is the pre-exponential factor,  $k_b$  is the Boltzmann constant and T is the temperature.

### **QENS Study**

Quasielastic neutron scattering (QENS) measures the small changes in a neutrons kinetic energy (neV - meV) that occur when they scatter from atoms in motion. In many cases, as with this sample, the inelastic scattering is dominated by incoherent scattering from hydrogen. The elastic peak is broadened through scattering from moving atoms, and the motion that hydrogen nuclei are undergoing may be interrogated by quantifying this broadening. Data collected over a range of momentum transfer vector (Q) can provide information about the geometry of motion and the rate of motion determines the extent of peak broadening.

Quasielastic neutron scattering experiments were carried out using the IRIS spectrometer in the PG002 configuration at the ISIS neutron and muon facility, UK. 1.3 g of hydrated sample was sealed inside an aluminium sample holder of annular geometry for data collection. Temperature was measured using RhFe resistance thermometers and controlled with a combination of a helium closed cycle refrigerator and electrically resistive heaters.

The resolution function of the instrument was measured using the sample cooled to base temperature (approx. 8 K), where any motion within the sample is assumed to be beyond the instrumental resolution. The sample was then heated to 353 K, with data collected in 10 K steps for approximately seven minutes. Data was accumulated for five times longer times at 253 and 293 K, with an extended run at 353 K. Data were recorded for 20, 100 and 600  $\mu\text{A}\cdot\text{h}$  of proton beam current.

IRIS has 51 spectroscopy detectors covering an angular range of 25-160°, which can be arbitrarily grouped to increase the signal to noise ratio at the expense of resolution in Q. Summing the signal of all detectors together can provide a rapid insight into the changing rate of dynamics, but greater collection times are needed to achieve the Q resolved data necessary to obtain insight into the geometry of motion.

The Q-resolved data collected at 353 K is shown in Figure S18. Each of the 51 detectors samples the same energy transfer range and thus has a unique value of Q for the elastic peak. Each spectrum was fitted with the convolution of the experimentally measured resolution function with a delta function to represent the elastic scattering and a 2 Lorentzian peaks, representing the inelastic broadening; a broad background representing motions too fast for quantification, such as molecular rotation and a narrower feature representing the diffusive hydrogen motion of interest. An example fit for one detector is shown in Figure 5 (main text).

**Table S1:** Crystal data and structure refinements for **PCM-1**.

Empirical formula	'C <sub>40</sub> H <sub>36</sub> Co N <sub>8</sub> O <sub>2</sub> '
Formula weight	719.70
Temperature(K)	100(1)
Radiation	Mo-K $\alpha$
Wavelength( $\lambda$ )	0.71073Å
Crystal system	Monoclinic
Space group	<i>C2/c</i>
<i>a</i> [Å]	17.465 (3)
<i>b</i> [Å]	11.465 (2)
<i>c</i> [Å]	24.566(5)
$\alpha$ [°]	90
$\beta$ [°]	93.87(3)
$\gamma$ [°]	90
Volume[Å <sup>3</sup> ]	4908.0(16)
<i>Z</i>	4
Density (calculated) [Mg/m <sup>3</sup> ]	0.947
F(000)	1500
Refl. used [ $I > 2\sigma(I)$ ]	4906
Independent reflections	5272
Refinement method	full-matrix least squares on $F^2$
GOF	1.065
Final <i>R</i> indices[ $I > 2\sigma(I)$ ]	$R_1 = 0.0868$ , $wR_2 = 0.2196$
<i>R</i> indices (all data)	$R_1 = 0.0903$ , $wR_2 = 0.2220$

**Table S2:** Selected Bond Distances (Å) and Bond Angles (°) in **PCM-1**.

Co1 – OW1	2.053(3)	Co – N3	2.157
Co1 – N1	2.171(3)	Co1 – N4	2.216(4)

OW1 – Co1 – OW1	179.35(15)	OW1 – Co1 – N1	91.56(11)
OW1 – Co1 – N3	90.33(8)	N3 – Co1 – N1	88.18(9)
OW1 – Co1 – N4	89.67(8)	N3 – Co1 – N4	180
N1 – Co1 – N4	91.82(9)	Co1 – OW1 – H1W1	128(4)

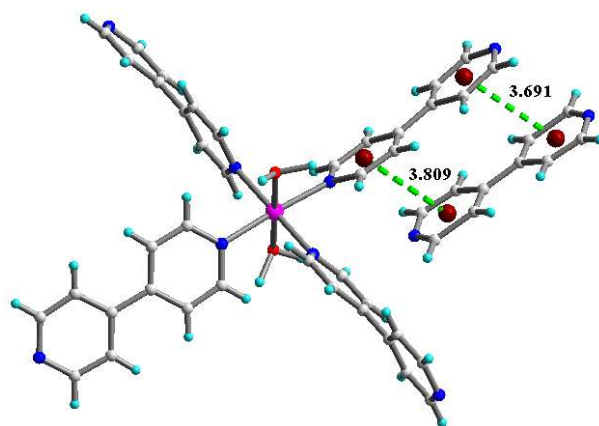


**Figure S1:** The  $\pi$ - $\pi$  interactions distance (in Å) between coordinated and non-coordinated bpy of **PCM-1**.

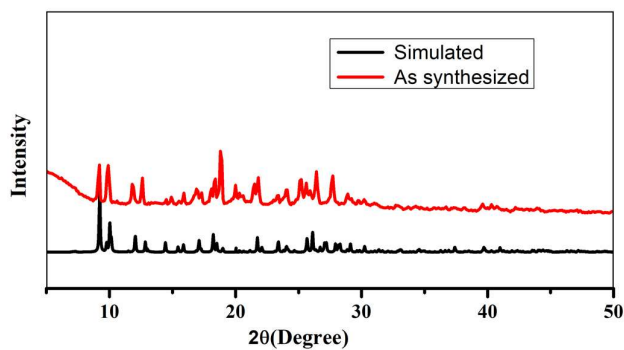


**Figure S2:** The PXRD pattern of simulated (black), as synthesized (red) of **PCM-1**.

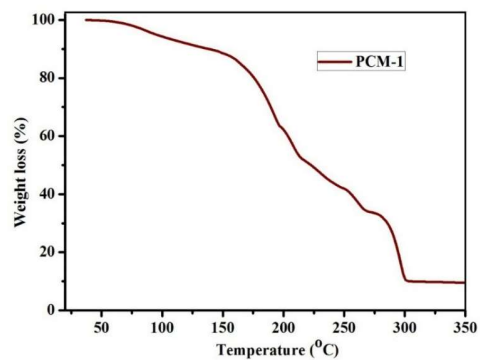


**Figure S3:** Thermo gravimetric analysis profile of **PCM-1**.

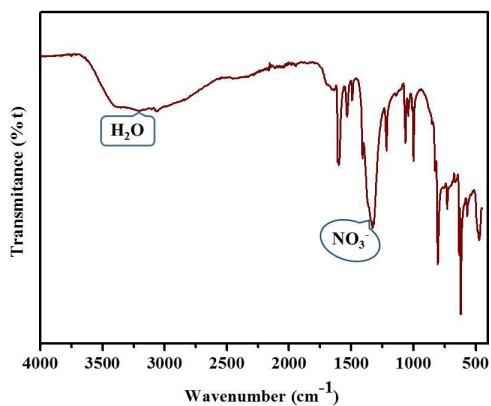


**Figure S4:** FTIR spectrum for **PCM-1**.

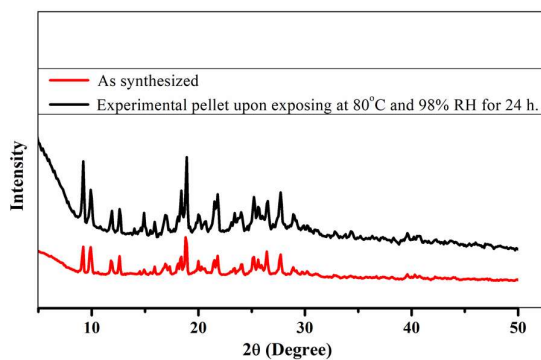


**Figure S5:** PXRD comparison of as synthesized (red) and pelleted (black) **PCM-1** after exposure to 98% R.H. at 80 °C for 24 h.

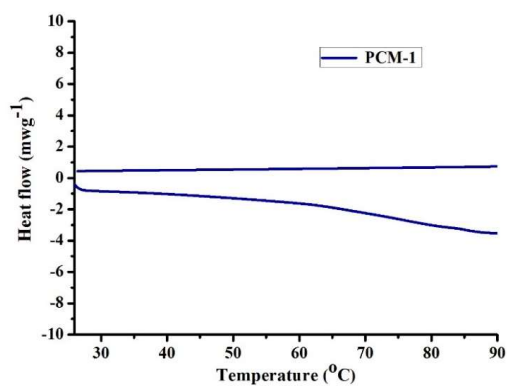


**Figure S6:** Differential scanning calorimetry for **PCM-1**.

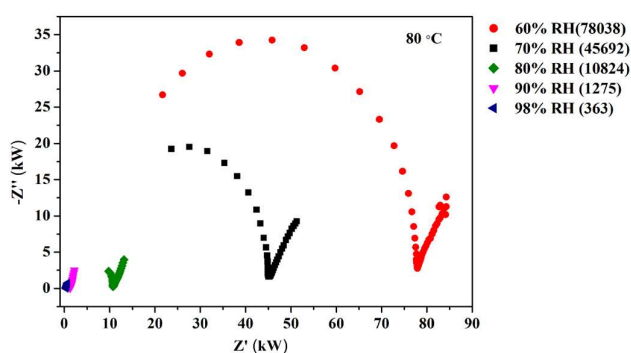


**Figure S7:** Nyquist plot of **PCM-1** at 80°C and 60% to 98% R.H. (resistance values in Ohm are given in parenthesis).

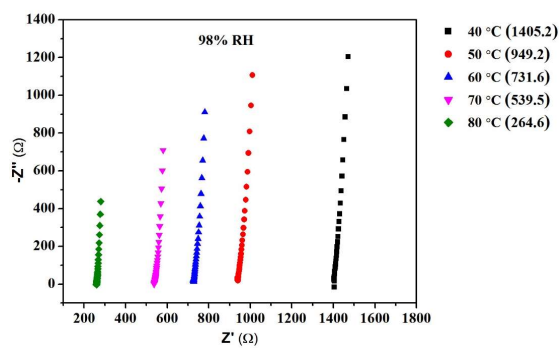


**Figure S8:** Nyquist plot of **PCM-1** at 98% R.H. and 40°C to 80°C temperature (resistance values in Ohm are given in parenthesis).

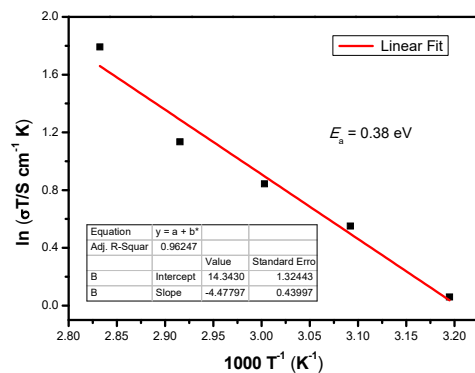


**Figure S9:** Arrhenius-type plots of  $\ln(\sigma T)$  vs.  $1000/T$  for **PCM-1** at R.H. of 98%.

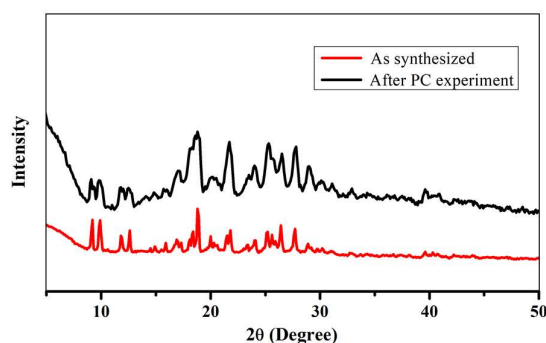


**Figure S10:** The PXRD pattern of as synthesized (red) and after proton conduction measurement (black) of **PCM-1**. The broadness is likely due to the reduced particle size. Such type of broadening of PXRD peaks after the proton conduction measurements could also be found for many well-known MOFs (a few representative examples: Kitagawa *et al. Chem. Mater.*, 2015, **27**, 2286–2289; Shimizu *et al. Chem. Mater.*, 2018, **30**, 314–318; Shimizu *et al. J. Am. Chem. Soc.*, 2013, **135**, 963–966, Shimizu *et al. J. Am. Chem. Soc.*, 2017, **139**, 14676–14683; Bu, and Feng *et al. Angew. Chem. Int. Ed.*, 2015, **54**, 7886–7890; Chen and Li *et al. Nat. Energy* 2017, **2**, 877–883; Shimizu *et al. Chem. Mater.*, 2020, **32**, 679–687; Xiang *et al. J. Mater. Chem. A*, 2016, **4**, 18742; Ghosh *et al. Angew. Chem. Int. Ed.*, 2014, **53**, 2638–2642; Zhou *et al. J. Am. Chem. Soc.*, 2017, **139**, 6183–6189). Nonetheless, the conductivity measurements until three cycles exhibit consistent values under extreme proton conduction measurement conditions.

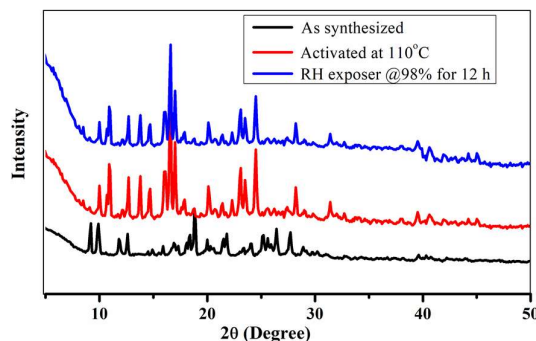


**Figure S11:** A representative PXRD pattern of as synthesized (black) and activated sample at 110 °C (red) of **PCM-1**. The sample was tested to activate in the temperature range of 60-110 °C under vacuum. From the above representative figure, it is clear that after activation PCM-1 changed to a different phase (red). While this activated phase is re-humidified at 98% RH, it did not return to the original phase, indicating that this transformation is irreversible in nature (blue). As the phase remained different from as synthesized one, water sorption measurement was not performed with this material.

## Molecular simulations

### Microscopic model for PCM-1

Since the positions of the  $\text{NO}_3^-$  groups were not experimentally determined, Monte Carlo simulations were performed in the NVT ensemble to determine the most probable location of these counter anions in the interspace among the 1D chains of the PCM-1. In this context, the interatomic CP/ $\text{NO}_3^-$  potential was modeled by considering van der Waals and electrostatic contributions described respectively by 12-6 Lennard-Jones (LJ) and Coulombic potentials. The LJ parameters ascribed to the atoms of the organic and inorganic nodes of the framework were taken from the Dreiding<sup>5</sup> and Universal<sup>6</sup> forcefields respectively. The atomic partial charges of the positive charged DFT-optimized PCM-1 framework without the  $\text{NO}_3^-$  groups were calculated using the REPEAT scheme<sup>7</sup> as implemented in the CP2K package. These atom types and their respective charges in **PCM-1** are listed in Table S3 and Figure S11. The nitrate groups were described using a previously derived model that was considered to deal with the ionic transport in narrow pores<sup>8</sup>. In this model  $\text{NO}_3^-$  is represented by atom-centered charged LJ sites with N-O bonds of 1.24 Å and a O-N-O angle of 122.9°. The total charge of the anion is -1. The so-obtained geometry optimized PCM-1 structures containing  $\text{NO}_3^-$  groups were further relaxed at the Density Functional Theory (DFT) level keeping the unit cell parameters fixed. In these calculations, the GGA-PBE functional<sup>9,10</sup> was combined with Gaussian basis sets and pseudopotentials as implemented in the CP2K package.<sup>11,12</sup>

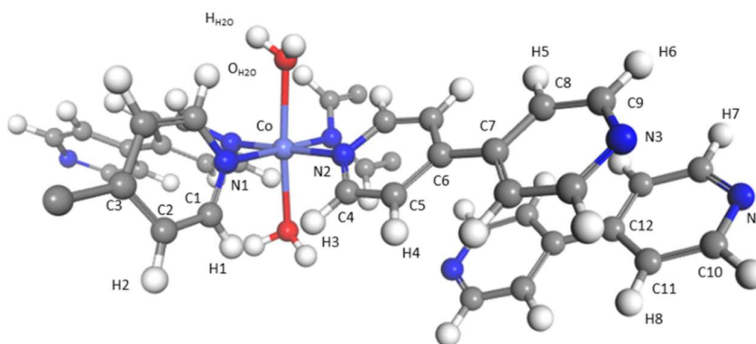


**Figure S12:** Atom types adopted in the description of the charges of the **PCM-1** structure.

The triple- $\zeta$  valence plus two polarization (TZV2P) basis set<sup>13</sup> was used for the H, O, N and C atoms, while Co was treated using the double- $\zeta$  valence plus polarization (DZVP) basis set.<sup>14</sup> The pseudopotentials used for all of the atoms were those derived by Goedecker, Teter, and Hutter.<sup>15,16</sup> A relative cutoff of 500 Ry and a convergence criterion for the self-consistent field interactions of  $10^{-6}$  were employed. The van der Waals interactions were considered via the use of semiempirical dispersion corrections as implemented in the DFT-D3 method.<sup>17</sup>

**Table S3:** REPEAT charges considered for each atom of the **PCM-1** network.

Atom type	Charge (au)	Atom type	Charge (au)
Co	0.5514	C12	0.4931
O <sub>H2O</sub>	-0.8276	N1	0.0763
H <sub>H2O</sub>	0.3890	N2	-0.0948
C1	-0.0130	N3	-0.5284
C2	-0.1813	N4	-0.6770
C3	0.1618	H1	0.1021
C4	0.0820	H2	0.1587
C5	-0.3993	H3	0.1076
C6	0.5376	H4	0.1848
C7	0.1575	H5	0.1793
C8	-0.4404	H6	0.0243
C9	0.4275	H7	0.0391
C10	0.4452	H8	0.2140
C11	-0.6067		

The most stable structural model (Figure S13) was further used for all the force field-based MC calculations in the presence of water.

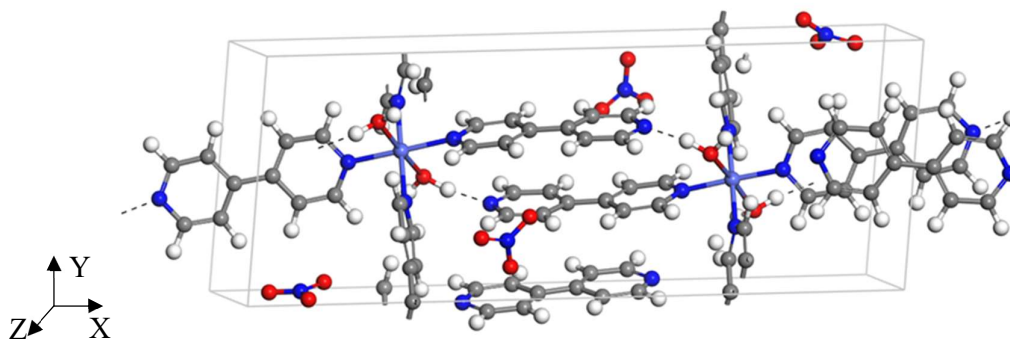


**Figure S13:** DFT optimized **PCM-1** framework evidencing the  $\pi$ - $\pi$  stacking of the coordinated and non-coordinated 4,4'-bpy linkers and the hydrogen bonds (black dashed lines) formed between neighbor coordinated water molecules and nitrogen atoms. In the y direction, the 4, 4'-bpy are double coordinated to Co(II) atoms, forming an infinite 1D. Meanwhile, in the x direction only a single coordination of the 4, 4'-bpy molecules is observed. Grey, white, red, deep and clear blue atom colors are respectively assigned to carbon, hydrogen, oxygen, nitrogen, and cobalt atoms.

### Monte Carlo simulations

Monte Carlo (MC) simulations were carried out in the Canonical (NVT) ensembles to explore the water adsorption behavior in **PCM-1** at room temperature. Water molecule was described by the 4-site model TIP4P/2005.<sup>18</sup> In complement to this, MC calculations were performed in the grand canonical ensemble to calculate the maximum theoretical loading and the enthalpy of adsorption ( $\Delta H_{\text{ads}}$ ) using the revised Windom insertion method.<sup>19</sup> The maximum loading obtained from these calculations was of about 18 molecules per unit cell (uc), In the NVT calculations, the number of adsorbed molecules in the system was progressively increased from a low uptake to the theoretical saturation ( $N_{\text{H}_2\text{O}} = 5, 8, 11, \text{ and } 18 \text{ mol./uc}$ ) to explore the arrangements of the water molecules at different hydration conditions. The  $\text{NO}_3^-$  molecules were allowed to move throughout the simulation box. The water/water, water/CP, water/  $\text{NO}_3^-$  and  $\text{NO}_3^-/\text{CP}$  interactions were treated as a sum of electrostatic and van der Waals interactions with crossed LJ parameters obtained by using a Lorentz-Berthelot combination rule.<sup>20</sup>

Radial distribution functions (RDFs) between diverse  $\text{H}_2\text{O}/\text{PCM-1}$  atom pairs, hydrogen bond network and cluster size analysis were performed to describe the structural topology of the water molecules in the pores of the material. The calculation of the hydrogen bonds was performed using two geometric criteria: distance between a donor (D) and an acceptor (A) atoms shorter than 3.5 Å and angle between the D-H vector and the D-A vector lower than 37°. These criteria are the same than those previously used to describe the H-bond network in other materials.<sup>21-24</sup> The analysis of the clusters of water molecules was based on

the definition of a cluster as a continuous network of water molecules. To define the aggregation of the water molecules in clusters, we defined a minimum mutual connectivity distance (RCL) between the oxygen atoms of neighboring H<sub>2</sub>O molecules. This value was defined as 3.1 Å to accurately represent the first interaction peak of the RDF O-O for liquid water.<sup>25</sup>

### Ab Initio Molecular Dynamic simulations

Born–Oppenheimer first-principles MD simulations with the consideration of an excess charge were performed for a single unit cell of **PCM-1** fully water saturated using the CP2K package and the same level of theory than the one used to geometry optimize the structure and extract the atomic partial charges. As in aqueous systems, the hydrogen bonding and proton shuffling and hopping phenomena occur in a time scale of only several femtoseconds and a few picoseconds, respectively<sup>26</sup>, these simulations were run with a time step of 1 fs for 10 ps at 298 K, in order to collect enough statistics to describe the main features of the microscopic proton conduction mechanism.

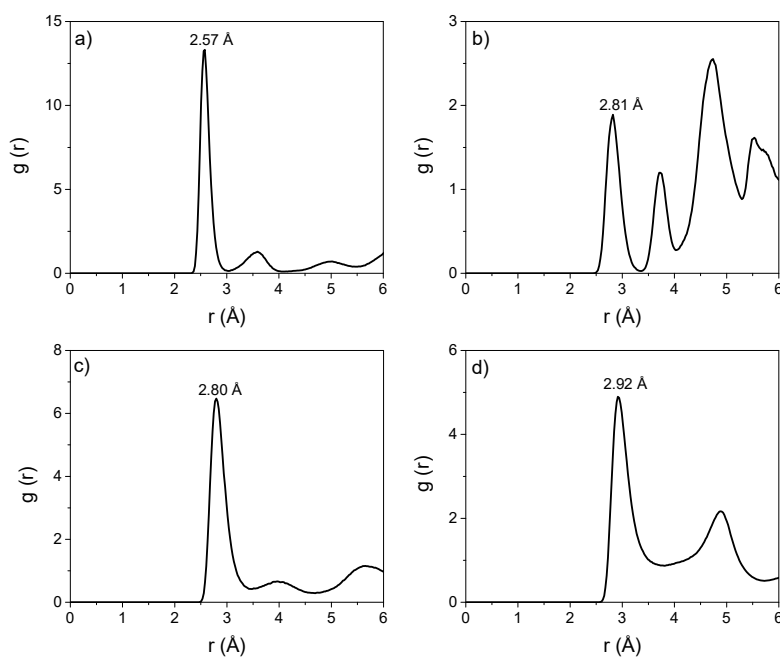


**Figure S14:** Radial distribution functions of the interactions between the pairs  $O_{H_2O_c} - O_w$  (a),  $N_{LIG} - O_w$  (b),  $OH_{2Ow} - OH_{2Ow}$  (c), and  $ONO_3^- - OH_{2Ow}$  (d) at  $N_{H_2O} = 5$ .

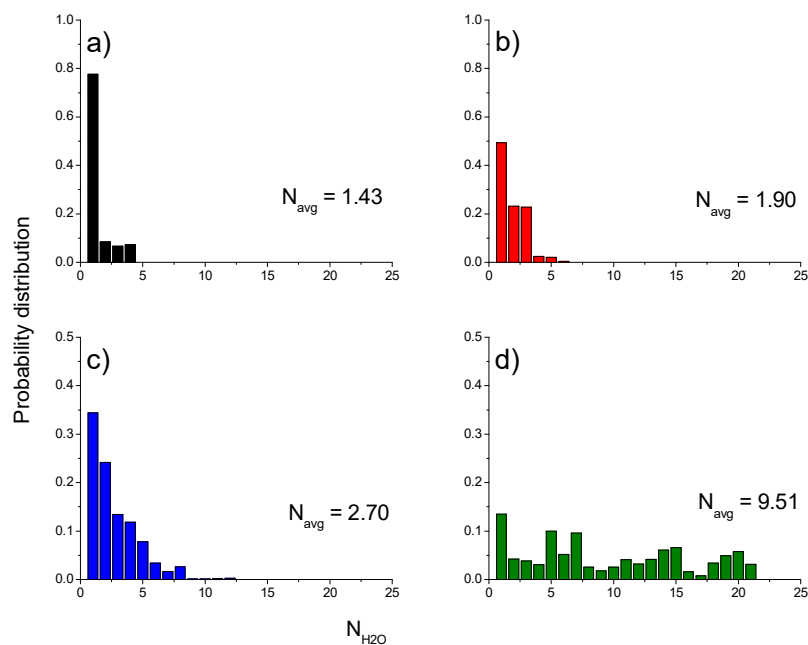


**Figure S15:** Evolution of the probability distribution of the water cluster sizes at different levels of hydration –  $N_{H_2O} = 5$  (a), 8 (b), 11 (c), and 18 (d) mol./uc – showing a clear increase in the average cluster size ( $N_{avg}$ ) with the water loading.

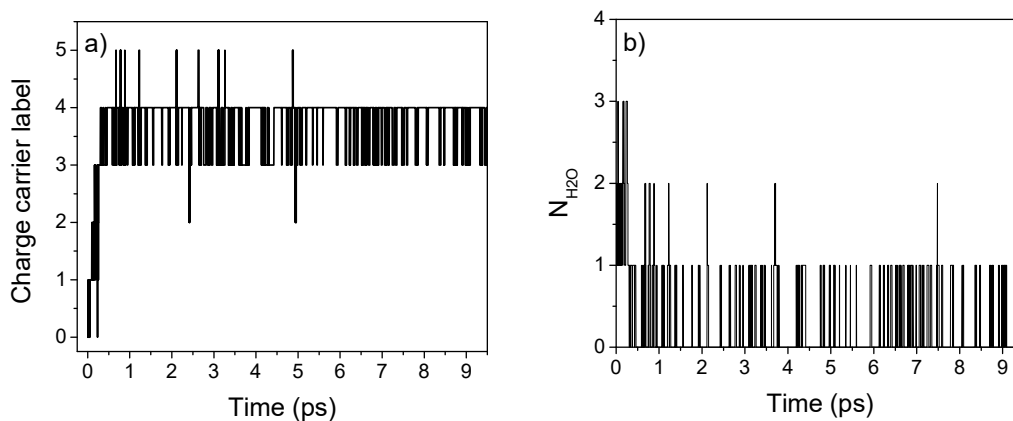


**Figure S16:** (a) Time evolution of the protonated indexed species calculated from the AIMD trajectory at 298 K. Indexes 1, 2, 3 and 5 are associated with hydronium species and index 4 corresponds to the  $HNO_3$  formed by the association of the excess proton and the  $NO_3^-$  groups. (b) Time evolution of the number of water molecules involved in the shuffling of the excess proton. The value 0, 1, 2 and 3 are respectively correlated to the formation of  $HNO_3$ ,  $H_3O^+$ ,  $H_5O_2^+$ , and  $H_7O_3^+$  species.

**Table S4:** Number of hydrogen bonds per adsorption site in PCM-1.

$N_{H_2O}$	$N_{H-bonds}/N_{NO_3^-}$	$N_{H-bonds}/N_{H_2O_c}$	$N_{H-bonds}/N_{Nlig}$
5	1.92	1.41	0.27
8	2.28	1.82	0.54
11	3.02	1.82	0.53
18	4.15	1.91	0.58

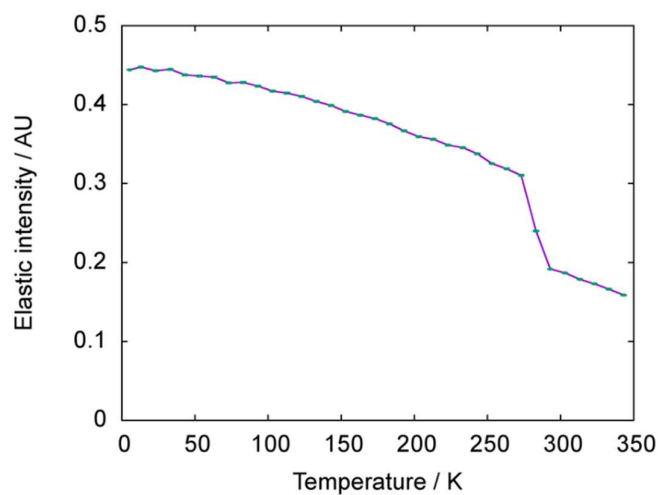


**Figure S17:** Fixed window scan showing the integrated elastic peak intensity as a function of temperature.

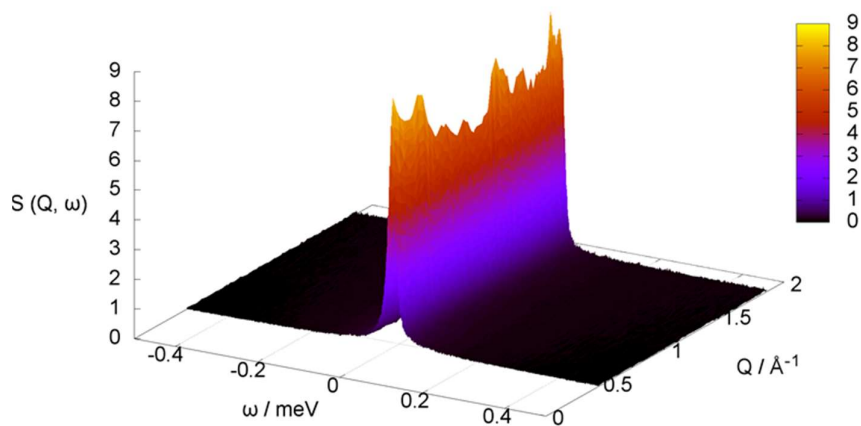


**Figure S18:** Quasielastic peak obtained at 353 K.

**Table S5:** Proton conduction values in descending order of reported materials up to  $10^{-3}$  S  $\text{cm}^{-1}$  range. Materials other than MOFs/CPs are indicated in parenthesis.

Compounds	Conductivity (S $\text{cm}^{-1}$ )	Conditions	$E_a$ (eV)	References
<b>PCM-1</b>	<b><math>1.85 \times 10^{-2}</math></b>	<b>80°C, 98% RH</b>	<b>0.38</b>	<b>This Work</b>
UiO-66(SO <sub>3</sub> H) <sub>2</sub>	$8.4 \times 10^{-2}$	80°C, 90% RH	0.32	<i>Angew. Chem. Int. Ed.</i> <b>2015</b> , <i>54</i> , 5142-5146
TfOH@MIL-101	$8.0 \times 10^{-2}$	60°C, 15% RH	0.23	<i>ACS Appl. Mater. Interfaces</i> <b>2014</b> , <i>6</i> , 5161 - 5167.
CPM-103a single crystal	$5.8 \times 10^{-2}$	22.5°C, 98% RH	0.66	<i>Angew. Chem.</i> <b>2015</b> , <i>127</i> , 7997 – 8001.
TJU-102	$5.26 \times 10^{-2}$	90 °C, 98% RH	0.59	<i>Chem. Mater.</i> <b>2019</b> , <i>31</i> , 8494–8503.
Fe-CAT-5	$5.0 \times 10^{-2}$	25°C, 98% RH	0.24	<i>J. Am. Chem. Soc.</i> <b>2015</b> , <i>137</i> , 15394 -15397.
PCMOF2(Pz)	$4.6 \times 10^{-2}$	85°C, 90% RH	0.10	<i>J. Am. Chem. Soc.</i> <b>2018</b> , <i>140</i> , 1077 –1082.
[(Me <sub>2</sub> NH <sub>2</sub> ) <sub>3</sub> (SO <sub>4</sub> ) <sub>2</sub> ][Zn <sub>2</sub> (ox) <sub>3</sub> ]	$4.2 \times 10^{-2}$	25°C, 98% RH	0.13	<i>Angew. Chem.</i> <b>2018</b> , <i>130</i> , 6772 –6776.
Co-tetra	$4.15 \times 10^{-2}$	80°C, 98% RH	0.29	<i>Angew. Chem.</i> <b>2018</b> , <i>130</i> , 6772 –6776.
[Co(DCDPP)]·5H <sub>2</sub> O	$3.90 \times 10^{-2}$	80°C, 97% RH	0.34	<i>J. Mater. Chem. A</i> <b>2017</b> , <i>5</i> , 14525 – 14529.
Mg <sub>2</sub> (H <sub>2</sub> O) <sub>4</sub> (H <sub>2</sub> L)·H <sub>2</sub> O (PCMOF-10)	$3.55 \times 10^{-2}$	70°C, 95% RH	0.45	<i>J. Am. Chem. Soc.</i> <b>2015</b> , <i>137</i> , 7640-7643
Im@MOF-808	$3.45 \times 10^{-2}$	65°C, 99% RH	0.25	<i>ACS Appl. Mater. Interfaces</i> <b>2019</b> , <i>11</i> , 9164–9171
[CuI-MOF@pz·6 HCl]	$2.94 \times 10^{-2}$	80°C, 95% RH	0.59	<i>Chem. Eur. J.</i> <b>2018</b> , <i>24</i> , 872– 880.
MIP-177-SO <sub>4</sub> H-LT	$2.6 \times 10^{-2}$	25°C, 95% RH	-	<i>ACS Sustainable Chem. Eng.</i> <b>2019</b> , <i>7</i> , 5776–5783
PCMOF <sub>2</sub> <sub>1/2</sub>	$2.1 \times 10^{-2}$	85°C, 90% RH	0.21	<i>J. Am. Chem. Soc.</i> <b>2013</b> , <i>135</i> , 963 –966.
KAUST-7'	$2.0 \times 10^{-2}$	90 °C, 95% RH	0.19	<i>J. Am. Chem. Soc.</i> <b>2018</b> , <i>140</i> , 13156–13160
Im@NENU-3	$1.82 \times 10^{-2}$	70 °C, 90% RH	0.57	<i>J. Am. Chem. Soc.</i> <b>2017</b> , <i>139</i> , 15604–15607
MROF-1	$1.72 \times 10^{-2}$	70°C, 97% RH	0.37	<i>J. Mater. Chem. A</i> <b>2016</b> , <i>4</i> , 18742– 18746.

Co-tetra	$1.38 \times 10^{-2}$	40°C, 98% RH	0.29	<i>Angew. Chem.</i> <b>2018</b> , <i>130</i> , 6772–6776.
(NH <sub>4</sub> ) <sub>2</sub> (adp)[Zn <sub>2</sub> (ox) <sub>3</sub> ]·3H <sub>2</sub> O	$1.64 \times 10^{-2}$	35°C, 98% RH	0.63	<i>J. Mater. Chem. A</i> <b>2016</b> , <i>4</i> , 16484-16489
VNU-15	$2.90 \times 10^{-2}$	95°C, 60% RH	0.22	<i>J. Mater. Chem. A</i> <b>2016</b> , <i>4</i> , 3638-3641.
Im@Fe–MOF	$1.21 \times 10^{-2}$	60°C, 98% RH	0.436	<i>J. Am. Chem. Soc.</i> <b>2017</b> , <i>139</i> , 6183-6189.
MIL-101-SO <sub>3</sub> H	$1.16 \times 10^{-2}$	80°C, 100% RH	0.23	<i>Nat. Energy</i> <b>2017</b> , <i>2</i> , 877 – 883.
MIP-202(Zr)	$1.1 \times 10^{-2}$	90°C, 95% RH	0.22	<i>Nat. Commun</i> <b>2018</b> , <i>9</i> , 4937.
(NH <sub>4</sub> ) <sub>2</sub> (H <sub>2</sub> adp)[Zn <sub>2</sub> (ox) <sub>3</sub> ]·3H <sub>2</sub> O	$8 \times 10^{-3}$	25 °C, 98% RH	0.63	<i>J. Am. Chem. Soc.</i> <b>2009</b> , <i>131</i> , 9906-9907.
HOF-GS-10	$7.5 \times 10^{-3}$	30 °C, 95% RH	0.49	<i>Angew. Chem. Int. Ed.</i> <b>2016</b> , <i>55</i> , 10667-10671.
Ca-PiPhtA-NH <sub>3</sub>	$6.6 \times 10^{-3}$	24 °C, 98% RH	0.40	<i>J. Am. Chem. Soc.</i> <b>2014</b> , <i>136</i> , 5731-5739.
PCMOF-5	$4.0 \times 10^{-3}$	62 °C, 98% RH	0.32	<i>J. Am. Chem. Soc.</i> <b>2013</b> , <i>135</i> , 1193-1196.
Cu–TCPP nanosheet	$3.9 \times 10^{-3}$	25 °C, 98% RH	0.28	<i>J. Am. Chem. Soc.</i> <b>2013</b> , <i>135</i> , 7438-7441.
Cd-5TIA	$3.61 \times 10^{-3}$	28 °C, 98% RH	0.16	<i>Chem. Commun.</i> <b>2012</b> , <i>48</i> , 5464-5466.
In-IA-2D-1	$3.4 \times 10^{-3}$	27 °C, 98% RH	0.61	<i>Chem. Commun.</i> <b>2013</b> , <i>49</i> , 6197-6199.
V <sup>II</sup> [Cr <sup>III</sup> (CN) <sub>6</sub> ] <sub>2/3</sub> ·4.2H <sub>2</sub> O	$2.6 \times 10^{-3}$	50 °C, 100% RH	0.10, 0.19	<i>J. Am. Chem. Soc.</i> <b>2010</b> , <i>132</i> , 6620-6621.
[{(Zn <sub>0.25</sub> ) <sub>8</sub> (O)}Zn <sub>6</sub> (L) <sub>12</sub> (H <sub>2</sub> O) <sub>2</sub> <sub>9</sub> (DMF) <sub>69</sub> (NO <sub>3</sub> ) <sub>2</sub> ] <sub>n</sub>	$2.3 \times 10^{-3}$	25 °C, 95% RH	0.22	<i>J. Am. Chem. Soc.</i> <b>2012</b> , <i>134</i> , 19432-19437.
(NH <sub>4</sub> ) <sub>4</sub> [MnCr <sub>2</sub> (ox) <sub>6</sub> ]·4H <sub>2</sub> O	$1.7 \times 10^{-3}$	40 °C, 96% RH	0.23	<i>J. Am. Chem. Soc.</i> <b>2011</b> , <i>133</i> , 15328-15331.
Co <sup>II</sup> [Cr <sup>III</sup> (CN) <sub>6</sub> ] <sub>2/3</sub> ·4.2H <sub>2</sub> O	$1.7 \times 10^{-3}$	35 °C, 100% RH	0.22	<i>J. Am. Chem. Soc.</i> <b>2010</b> , <i>132</i> , 6620-6621.
NENU-530	$1.5 \times 10^{-3}$	75 °C, 98% RH	0.33	<i>Chem. Eur. J.</i> , <b>2016</b> , <i>22</i> , 9299
MgH <sub>6</sub> ODTMP·6H <sub>2</sub> O	$1.5 \times 10^{-3}$	19 °C, 100% RH	0.31	<i>Inorg. Chem.</i> <b>2012</b> , <i>51</i> , 7689-7698.
β-PCMOF2	$1.3 \times 10^{-3}$	85 °C, 90% RH	0.28	<i>J. Am. Chem. Soc.</i> <b>2013</b> , <i>135</i> , 963-966.
Fe(Ox)·2H <sub>2</sub> O	$1.3 \times 10^{-3}$	25 °C, 98% RH	0.37	<i>J. Am. Chem. Soc.</i> <b>2009</b> , <i>131</i> , 3144-3145.

## References:

- (1) SAINT+, 6.02ed, Bruker AXS, Madison, WI, **1999**.
- (2) XPREP, 5.1 ed. Siemens Industrial Automation Inc., Madison, WI, **1995**.
- (3) G. M. Sheldrick, *Acta Cryst C*, **2015**, *71*, 3–8.
- (4) A. L. Spek, *J. Appl. Crystallogr.* **2003**, *36*, 7–13.
- (5) S. L. Mayo, B. D. Olafson, W. A. Goddard III, *J. Phys. Chem.* **1990**, *94*, 8897–8909.
- (6) A. K. Rappe, C. J. Casewit, K. S. Colwell, W. A. Goddard III, W. M. Skiff, *J. Am. Chem. Soc.* **1992**, *114*, 10024–10035.
- (7) C. Campaña, B. Mussard, T. K. Woo, *J. Chem. Theory Comput.* **2009**, *5*, 2866–2878.
- (8) L. A. Richards, A. I. Schäfer, B. S. Richards, B. Corry, *Small* **2012**, *8*, 1701–1709.
- (9) J. P. Perdew, K. Burke, M. Ernzerhof, *Phys. Rev. Lett.* **1996**, *77*, 3865–3868.
- (10) J. P. Perdew, K. Burke, M. Ernzerhof, *Phys. Rev. Lett.* **1997**, *78*, 1396.
- (11) J. VandeVondele, M. Krack, F. Mohamed, M. Parrinello, T. Chassaing, J. Hutter, *Phys. Commun.* **2005**, *167*, 103–128.
- (12) J. Hutter, M. Iannuzzi, F. Schiffmann, J. VandeVondele, *Wiley Interdiscip. Rev. Comput. Mol. Sci.* **2014**, *4*, 15–25.
- (13) F. Weigend, R. Ahlrichs, *Chem. Chem. Phys.* **2005**, *7*, 3297.
- (14) M. Krack, *Theor. Chem. Acc.* **2005**, *114*, 145–152.
- (15) S. Goedecker, M. Teter, J. Hutter, *Phys. Rev. B* **1996**, *54*, 1703–1710.
- (16) C. Hartwigsen, S. Goedecker, J. Hutter, *Phys. Rev. B* **1998**, *58*, 3641–3662.
- (17) S. Grimme, J. Antony, S. Ehrlich, H. Krieg, *J. Chem. Phys.* **2010**, *132*, 154104.
- (18) J. L.F. Abascal, C. Vega, *J. Chem. Phys.* **2005**, *123*, 234505.
- (19) T. J. H. Vlugt, E. García-Pérez, D. Dubbeldam, S. Ban, S. Calero, *J. Chem. Theory Comput.* **2008**, *4* 7, 1107–1118.
- (20) H. A. Lorentz, *Ann. Phys.* **1881**, *248*, 127–136.
- (21) D. D. Borges, S. Devautour-Vinot, H. Jobic, J. Ollivier, F. Nouar, R. Semino, T. Devic, C. Serre, F. Paesani, G. Maurin, *Angew. Chemie Int. Ed.* **2016**, *55*, 3919–3924.
- (22) P. G. M. Mileo, S. Devautour-Vinot, G. Mouchaham, F. Faucher, N. Guillou, A. Vimont, C. Serre, G. Maurin, *J. Phys. Chem. C* **2016**, *120*, 24503–24510.
- (23) P. G. M. Mileo, T. Kundu, R. Semino, V. Benoit, N. Steunou, P. L. Llewellyn, C. Serre, G. Maurin, S. Devautour-Vinot, *Chem. Mater.* **2017**, *29*, 7263–7271.
- (24) P. G. M. Mileo, K. Adil, L. Davis, A. Cadiau, Y. Belmabkhout, H. Aggarwal, G. Maurin, M. Eddaoudi, S. Devautour-Vinot, *J. Am. Chem. Soc.* **2018**, *140*, 13156–13160.
- (25) W. L. Jorgensen, *Chem. Phys. Lett.* **1980**, *70*, 326–329.
- (26) O. Markovitch, H. Chen, S. Izvekov, F. Paesani, G. A. Voth, N. Agmon, *J. Phys. Chem. B* **2008**, *112*, 9456–9466.